Influence of homogeneous magnetic fields on the flow of a ferrofluid in the Taylor-Couette system

S. Altmeyer, Ch. Hoffmann, A. Leschhorn, and M. Lücke

Institut für Theoretische Physik, Universität des Saarlandes, D-66123 Saarbrücken, Germany

We investigate numerically the influence of a homogeneous magnetic field on a ferrofluid in the gap between two concentric, independently rotating cylinders. The full Navier-Stokes equations are solved with a combination of a finite difference method and a Galerkin method. Structure, dynamics, symmetry properties, bifurcation, and stability behavior of different vortex structures are investigated for axial and transversal magnetic fields, as well as combinations of them. We show that a transversal magnetic field modulates the Taylor vortex flow and the spiral vortex flow. Thus, a transversal magnetic field induces wavy structures: wavy Taylor vortex flow (wTVF) and wavy spiral vortex flow. In contrast to the classic wTVF, which is a secondarily bifurcating structure, these magnetically generated wavy Taylor vortices are pinned by the magnetic field, i.e., they are stationary and they appear via a primary forward bifurcation out of the basic state of circular Couette flow.

I. INTRODUCTION

The Taylor-Couette system has been the subject of research activities for many decades [1–8]. This simple model system is used for measurements of some hydrodynamic properties of fluids as well as for basic research in hydrodynamics, bifurcation mechanisms and pattern formation.

One of the many fascinating features of ferrofluids is the influence on the macroscopic flow by a magnetic field and vice versa [9–14]. One famous effect of this interaction is the dependence of the rotational viscosity of a ferrofluid on a magnetic field, the so-called magnetoviscous effect [15–18]. Quantitative investigations of the magnetoviscous effect are very important for technical applications. One method to quantify the rotational viscosity is the measurement of the critical angular velocity in the Taylor-Couette system [19–22]. From the more theoretical point of view, there is the question of how far the introduction of an additional force such as the magnetic one influences bifurcations and pattern formation.

In the literature, one can find many theoretical works that analyze the influence of rotational symmetric magnetic fields, i.e., axial, azimuthal, and radial ones on the flow of a ferrofluid in the Taylor-Couette system [14,23–29]. Odenbach and Müller [30] investigated the off-equilibrium magnetization of a ferrofluid in the Taylor-Couette system in a homogeneous transversal magnetic field. In this paper we present numerical calculations for different homogeneous magnetic fields. We focus on pure symmetric axial fields, pure transversal fields, and superpositions of both.

Transversal fields break the rotational symmetry. The advantage of such a field configuration is that it is relatively simple to realize such homogeneous magnetic fields in an experimental setup [30]. This fact allows to check our results by experiments. Otherwise, the breaking of the rotational symmetry by the transversal field generates several new nonlinearly driven effects which are compared with the influence of the axial field. The latter mainly stabilizes [14] the basic state of circular Couette flow (CCF) [31].

Furthermore, a transversal magnetic field component modulates pure structures such as Taylor vortex flow (TVF)

and spiral vortex flow (SPI) generating so called wavy Taylor vortices (wTVF) and wavy spiral vortices (wSPI), respectively, which differ crucially from the classical ones without magnetic fields [32–35]. This seems to be the first time that stable forward bifurcating wavy structures out of the basic state were seen. Moreover, wTVF without any azimuthal rotation is observed.

We elucidate differences and similarities of wavy structures generated with and without magnetic fields by investigating their Fourier spectra as well as their frequencies.

In Sec. II, we describe the system and our methods of investigation. There we present the field equations for the magnetization and the velocity field and we describe implications of the presence of the magnetic terms in the generalized Navier-Stokes equations. This is followed by Sec. III presenting our main results. Therein we elucidate how the different structures of (w)TVF and (w)SPI are influenced by a pure axial, a pure transversal, or an oblique field. We focus on bifurcation properties, stability, and spatiotemporal dynamics of the involved flow states. In the first part of Sec. III the bifurcation behavior, depending on different magnetic fields, of (w)TVF and (w)SPI is discussed. The second part presents the differences between the involved flow states with and without any magnetic field.

II. SYSTEM AND THEORETICAL DESCRIPTION

The Taylor-Couette system (Fig. 1) consists of two concentric, independently rotating cylinders (rotation rates $\Omega_1 > 0$ and Ω_2) with no-slip boundary conditions at the cylinder surfaces with the radii r_1 and $r_2 > r_1$. Here we consider periodic boundary conditions in axial direction with periodicity length Γ. The gap between the cylinders is filled with a viscous, incompressible, and isothermal ferrofluid in a homogeneous magnetic field

$$\mathbf{H} = H_x \mathbf{e}_x + H_z \mathbf{e}_z \qquad (2.1)$$

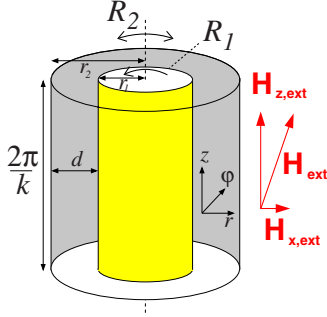with an axial component H_z and a transversal component H_x.

FIG. 1. (Color online) Schematic sketch of the Taylor-Couette system in a homogeneous magnetic field $\mathbf{H}_{ext}$.

The flow field

$$\mathbf{u} = u\mathbf{e}_r + v\mathbf{e}_\varphi + w\mathbf{e}_z \qquad (2.2)$$

is decomposed into a radial part u, an azimuthal component v, and an axial one w.

A. Magnetization equations

A variety of models which describe the magnetization dynamics in ferrofluids are discussed in the literature. Most of them either use the relaxation of the magnetization $\mathbf{M}$ into the equilibrium magnetization

$$\mathbf{M}_{eq} = M_{eq}(H)\mathbf{H}/H \qquad (2.3)$$

or they use the relaxation of an effective field

$$\mathbf{H}_{eff} = M_{eq}^{-1}(M)\mathbf{M}/M \qquad (2.4)$$

into the magnetic field $\mathbf{H}$ both with one single relaxation time [9,10,18,36–41]. In the stationary case, these relaxation equations have the common form [42]

$$(\mathbf{\Omega} + \kappa\mathbf{M} \times \mathbf{H}) \times \mathbf{M} = \gamma_\tau(\mathbf{M} - \gamma_\chi\mathbf{H}) \qquad (2.5)$$

with $\mathbf{\Omega} = \frac{1}{2}\nabla \times \mathbf{u}$ being the local vorticity. The coefficients κ, γ_τ, and γ_χ which differ from model to model are functions of H, M, and of some material properties of the ferrofluid.

A model reflecting the fact that real ferrofluids contain magnetic particles of different size considers the ferrofluid as a mixture of ideal monodisperse paramagnetic fluids [43,44]. Then, the resulting magnetization is given by $\mathbf{M} = \Sigma\mathbf{M}_j$ where $\mathbf{M}_j$ denotes the magnetization of the particles with diameter D_j. Each submagnetization $\mathbf{M}_j$ is assumed to obey a simple Debye relaxation dynamics described by

$$d_t\mathbf{M}_j = \mathbf{\Omega} \times \mathbf{M}_j - \frac{1}{\tau_j}(\mathbf{M}_j - \mathbf{M}_j^{eq}). \qquad (2.6)$$

Here, $\mathbf{M}_j^{eq}$ denote the equilibrium submagnetizations, τ_j the effective relaxation times of the different particle species.

We used for our numerical calculations an approach analogous to the model of Niklas *et al.* [24,26]. Therefore, we assumed a stationary magnetization near equilibrium with small $|\mathbf{M} - \mathbf{M}^{eq}|$ and small relaxation times, $\Omega\gamma_\tau^{-1} \ll 1$ resp. $\Omega\tau_j \ll 1$. In this case Eq. (2.5) and (2.6) can be simplified to

$$\mathbf{M} - \mathbf{M}^{eq} = c_N\mathbf{\Omega} \times \mathbf{H} \qquad (2.7)$$

with

$$c_N = \frac{\gamma_\chi}{\gamma_\tau + \kappa\gamma_\chi H^2} \quad \text{resp.} \quad c_N = \sum_j \chi_j\tau_j. \qquad (2.8)$$

B. Navier-Stokes equations

For an incompressible ferrofluid with kinematic viscosity ν the continuity equation and the Navier-Stokes equations read

$$0 = \nabla \cdot \mathbf{u} \qquad (2.9)$$

$$(\partial_t + \mathbf{u} \cdot \nabla)\mathbf{u} = \nabla^2\mathbf{u} - \nabla p + 2(\mathbf{M} \cdot \nabla)\mathbf{H} + \nabla \times (\mathbf{M} \times \mathbf{H}). \qquad (2.10)$$

Here, lengths are scaled by the gap width $d = r_2 - r_1$, time by the diffusion time d^2/ν, velocities with ν/d, the pressure with $\rho\nu^2/d^2$, and the magnetic field $\mathbf{H}$ and the magnetization $\mathbf{M}$ with $\sqrt{2\rho/\mu_0}\nu/d$ [28]. By means of Eq. (2.7), the magnetization can be eliminated in Eq. (2.10) so that

$$(\partial_t + \mathbf{u} \cdot \nabla)\mathbf{u} = \nabla^2\mathbf{u} - \nabla p_M + (\nabla c_N) \times (\mathbf{F} \times \mathbf{H})$$
$$+ c_N[\mathbf{F}(\nabla \cdot \mathbf{H}) - \mathbf{H}(\nabla \cdot \mathbf{F}) - \mathbf{H} \times (\nabla \times \mathbf{F})] \qquad (2.11)$$

with $\mathbf{F} = \mathbf{\Omega} \times \mathbf{H}$. p_M combines the pressure p as well as all magnetic terms which can be written as a gradient.

In a first approach, we assume the *internal* magnetic field to be equal to the *externally* imposed magnetic field $\mathbf{H} = \mathbf{H}_{ext}$ [c.f. Eq. (2.1)]. Then, Eq. (2.11) can be simplified to

$$(\partial_t + \mathbf{u} \cdot \nabla)\mathbf{u} = (1 + s_N^2)\nabla^2\mathbf{u} - \nabla p_M - \mathbf{s}_N \times \nabla[(\nabla \times \mathbf{u}) \cdot \mathbf{s}_N]. \qquad (2.12)$$

In this approach, the magnetic field and all the magnetic properties of the ferrofluid influence the velocity field only via the magnetic field parameter

$$\mathbf{s}_N = s_x\mathbf{e}_x + s_z\mathbf{e}_z = \sqrt{\frac{c_N}{2}}\mathbf{H}. \qquad (2.13)$$

In Fig. 2 we illustrate the dependence of this parameter on the magnetic field as well as the influence of the used magnetization model. Therefore, we calculated the absolute value $|\mathbf{s}_N(H)|$ by using a simple Debye-model ($\gamma_\chi = \chi, \gamma_\tau = \tau^{-1}, \kappa = 0$) [14], the polydisperse Debye-model Eq. (2.6), and a model introduced by Shliomis *et al.* [18] [$\gamma_\chi = \chi, \gamma_\tau = \tau^{-1}, \kappa = \mu_0/(6\Phi\nu\rho)$]—respectively, denoted as DEBYE, POLY and S72 [14]. We use the material parameters of the commercial ferrofluid APG933 and of a ferrofluid used in recent experiments [22].

C. Numerical method

The Navier-Stokes Eq. (2.12) that is augmented by the additional magnetic terms of our approach are solved numerically with the code G1D3 presented in [45,46]. G1D3 combines a finite difference method in $r - z$ plane and time with spectral decomposition in φ direction
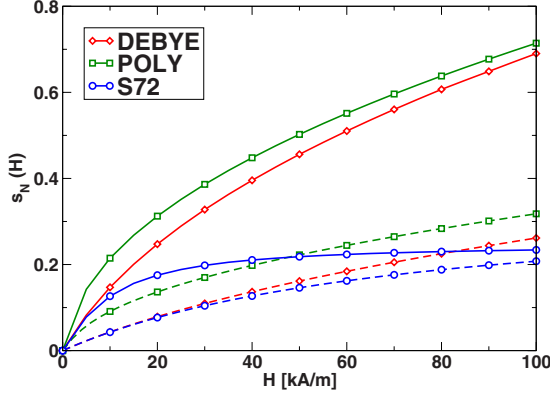
FIG. 2. (Color online) Variation of the absolute value $s_N(H)$ of the magnetic field parameter $\mathbf{s}_N(H)$ [Eqs. (2.8) and (2.13)] with H. Curves refer to the models DEBYE, POLY, and S72 [14]. Parameters of the commercial ferrofluid APG933 (full line) and of a ferrofluid used in recent experiments [22] (dashed).

$$f(r,\varphi,z,t) = \sum_{m=-m_{\max}}^{m_{\max}} f_m(r,z,t)e^{im\varphi}. \qquad (2.14)$$

Here f denotes one of $\{u,v,w,p\}$. We choose $m_{\max}=8$ for an adequate accuracy. For diagnostic purposes we also evaluate the complex mode amplitudes $f_{m,n}(r,t)$ obtained from a Fourier decomposition in axial direction

$$f_m(r,z,t) = \sum_n f_{m,n}(r,t)e^{inkz}. \qquad (2.15)$$

Here $k=2\pi/\lambda$ is the wave number and $\lambda=\Gamma$ is the wavelength. Beside this we also used a shooting method for calculations of linear stability boundaries [14].

D. Classification of the investigated structures

At not too high values of Ω_1, the velocity field in the ferrofluid is given by the circular Couette flow

$$\mathbf{u}_{CCF} = (A_{CCF}r + B_{CCF}r^{-1})\mathbf{e}_\varphi. \qquad (2.16)$$

The no-slip boundary conditions $\mathbf{u}(r_i)=\Omega_i r_i \mathbf{e}_\varphi (i=1,2)$ yield the coefficients $A_{CCF}=\frac{R_2-\eta R_1}{1+\eta}$ and $B_{CCF}=\frac{\eta(R_1-\eta R_2)}{(1-\eta)^2(1+\eta)}$ with the Reynolds numbers $R_i=\Omega_i r_i \frac{d}{\nu}$ and the radii ratio $\eta=r_1/r_2$.

In the following we give a short overview of the different supercritical flow patterns that we investigate in this paper: We investigate toroidally closed as well as helical vortex structures. Pure structures, Taylor vortices (●) and spiral vortices (▲) are calculated, as well as their modulated variants, so called wavy structures, i.e., wavy Taylor vortices (■) and wavy spiral vortices (◆). All these structures will be presented in the following by their corresponding symbols. The wavy structures are topologically identical with the pure states, but they show a wavy-like deformation that results from additional and other stimulated modes compared to the pure structures. In Sec. II E, we discuss in detail which modes are stimulated by different imposed magnetic fields.

The magnetically generated wTVF dramatically differs from the classic wTVF without any applied magnetic field that can be found in the literature [32–35]. The magnetically
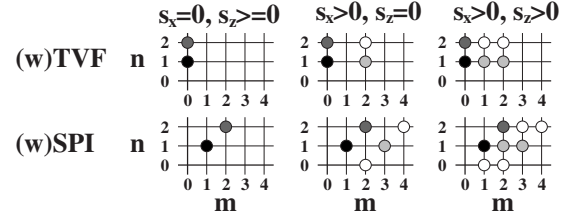

FIG. 3. Schematic sketch of modes in the presence of different externally imposed magnetic fields. Here m represents the azimuthal, and n the axial mode index in the expansion [Eqs. (2.14) and (2.15)]. Left row: modes without magnetic field or in a pure axial magnetic field. Middle row: pure transversal magnetic field. Right row: superposition of axial and transversal fields. The magnitudes are characterized by circles as follow: Black > dark grey > bright grey > white. For more details see text, and for numerical calculations see also Fig. 8.

induced wTVF are nonrotating structures having a *pinned phase*, whereas the classic wTVF rotate azimuthally. The imposed magnetic field shrinks the vortices at constant φ positions and expands them at others (see Sec. III E).

E. Mode coupling–stimulated modes in magnetic fields

The magnetic terms in the Navier-Stokes Eq. (2.12) induce many new phenomena. In particular, additional modes are stimulated by magnetic fields with a transversal component. In Fig. 3 we present a schematic plot for the stimulated modes depending on different external **H**-fields.

A pure axial field ($s_x=0, s_z>0$) does not stimulate any additional modes. Thus, TVF still contains only the modes $m=0, n\neq0$. On the other hand, e.g., a L1-SPI, i.e., a lefthanded SPI flow with azimuthal wave number 1 contains modes on the diagonal $m=n$. Thus, the mode spectra of TVF and SPI does not change qualitatively when a pure axial field is applied.

However, for $s_x>0, s_z=0$ the magnetic field excites $m=\pm2$ modes in wTVF and in wSPI modes lying on the secondary diagonal $m=n+2$ are stimulated. Thus, the pure TVF and SPI structures do not exist anymore in the presence of a transversal magnetic field. If the magnetic field has an axial and a transversal component ($s_x>0, s_z>0$) in addition to the case $s_x=0, s_z>0$ also $m=\pm1$ modes appear in wTVF. In wSPI one additionally observes modes on the diagonal $m=n+1$ as indicated in the right column of Fig. 3. The magnitudes of the magnetically stimulated modes depend on the applied fields. They are illustrated in Fig. 3 by different circles (see caption). Moreover, the additional modes can induce further nonlinear mode-couplings, too. Thus, the mode spectra become very complex. For numerical calculations see also Fig. 8. The bifurcation behavior and the structure of these vortex flows are discussed further below.

III. RESULTS

A. Bifurcation behavior

We already mentioned that magnetic fields tend to shift the onset for vortex flow and stabilize the basic state. But
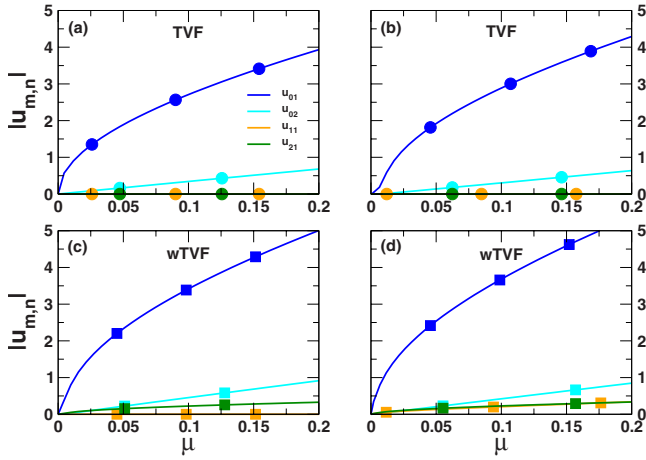
FIG. 4. (Color online) Bifurcation diagrams of TVF (●) and wTVF (■) in different magnetic fields: (a) $s_x=0=s_z$, (b) $s_x=0, s_z=0.6$, (c) $s_x=0.6, s_z=0$, (d) $s_x=0.6, s_z=0.6$. Moduli $|u_{m,n}|$ of the radial flow field amplitudes at mid gap are shown versus the relative distance μ (3.1) from the onset of the respective vortex flow. Parameters are $\eta=0.5$, $k=3.927$, $R_2=0$. In the case of a finite transversal field component in (c) and (d), new modes become stimulated as illustrated in Fig. 3. Symbols in this and all other figures are to guide the eyes. Calculations have been done for many more control parameters.

first of all we will focus on the bifurcation behavior of the different structures with the additionally field induced modes that are explained in Sec. II E.

In Fig. 4 the stable forward bifurcating branches of TVF and of wTVF solutions are presented for different imposed **H**-fields. Figure 5 shows the bifurcation diagrams for SPI and wSPI in an analogous way. For easier comparison of the bifurcation branches, we take as control parameter the relative distance
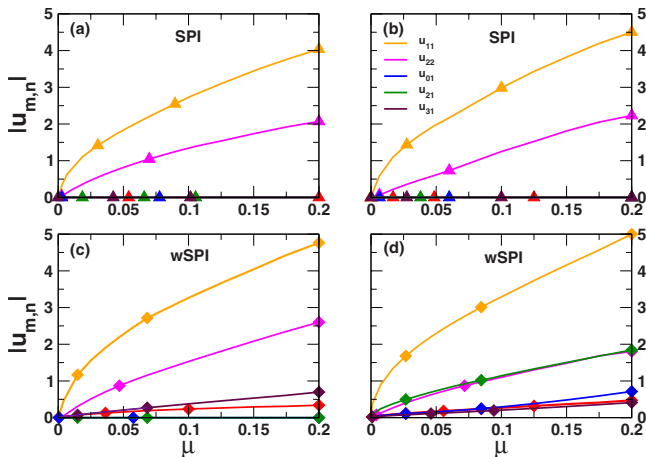

FIG. 5. (Color online) Bifurcation diagrams of SPI (▲) and wSPI (◆) in different magnetic fields: (a) $s_x=0=s_z$, (b) $s_x=0, s_z=0.6$, (c) $s_x=0.6, s_z=0$, (d) $s_x=0.6, s_z=0.6$. Moduli $|u_{m,n}|$ of the radial flow field amplitudes at mid gap are shown versus the relative distance μ Eq. (3.1) from the onset of the respective vortex flow. Parameters are $\eta=0.5$, $k=3.927$, $R_2=-150$. In the case of a finite transversal field component in (c) and (d) new modes become stimulated as illustrated in Fig. 3.

$$\mu = \frac{R_1}{R_{1,bif}(s_x, s_z)} - 1 \qquad (3.1)$$

of R_1 to the bifurcation threshold $R_{1,bif}(s_x, s_z)$ for the vortex flow in question in the respective magnetic field.

In order to characterize the structures, we display first of all the dominant as well as the first higher harmonic mode of the corresponding structure, e.g., (0,1) and (0,2) for TVF. In addition, the largest field-induced mode amplitudes of the wavy structures (c.f. Figure 3) are included for comparison. The symbols in Figs. 4 and 5 and in all other figures are plotted to guide the eyes: numerical calculations have been done for many more parameters.

1. Axial field

A pure axial **H**-field ($s_x=0, s_z\neq0$) does not change the structure of TVF and SPI qualitatively. Both vortex flows remain as they are without field since no additional modes are stimulated by an axial field, c.f. the first row in Fig. 3. The only, but important effect is the shift of the onsets to higher values of R_1 [14]. For example, the onset of TVF is shifted upwards by about 24% for the parameters of Fig. 4(b) and the SPI bifurcation threshold moves upwards in R_1 by about 15% for the parameters of Fig. 5(b), c.f. Sec. III D. Also the frequencies of SPI are increased in an axial field, c.f. Sec. III F.

2. Transversal field

On the other hand, a finite transversal **H**-field ($s_x \neq 0$) has a more dramatic influence on TVF and SPI: it not only delays their onset but it also changes their structure. In the case of TVF the application of a transverse field stimulates modes with azimuthal mode index $m= \pm 2$, c.f. upper center part of Fig. 3. The variation of the modulus $|u_{2,1}|$ with μ is contained in Fig. 4(c). In the case of an original L1-SPI the transversal field generates additional modes with indices $m=n+2$, c.f. lower center part of Fig. 3. The modulus $|u_{3,1}|$ is shown in Fig. 5(c). Note that also the $(1,-1)$ mode gets excited that represents a small admixture of a R1-SPI.

Thus, in a magnetic field with a finite transversal component the pure TVF and SPI structures do not exist any more. Instead, wavy vortices bifurcate as primary structured solutions forward out of the CCF ground state; namely wavy Taylor vortices in Figs. 4(c) and 4(d) or wavy spirals in Figs. 5(c) and 5(d).

The stabilization of the CCF by a transversal magnetic field is a bit smaller than by an axial one of the same magnitude: the upwards shift for the onset of wTVF (wSPI) in a transversal field is about 21% (13%) smaller than the corresponding shift for the TVF (SPI) bifurcation threshold in an axial magnetic field.

3. Oblique field

In comparison with the pure field cases, $s_x=0$ or $s_z=0$, the onset of wTVF and WSPI in a **H**-field that is oriented obliquely to the cylinder ($s_x \neq 0 \neq s_z$) is shifted to higher values. Furthermore, such a superposition of an axial and a transver-
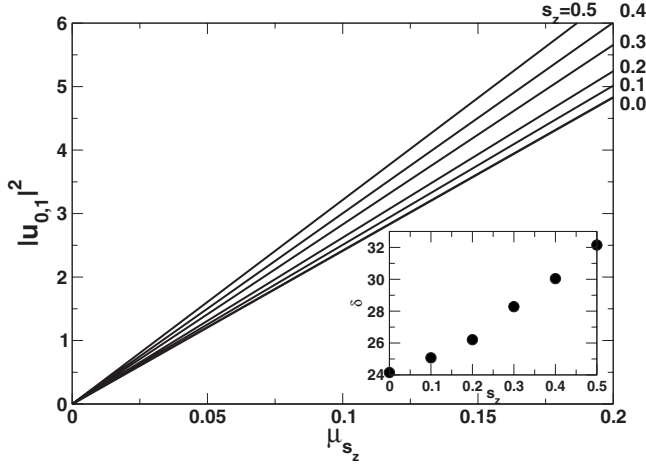
FIG. 6. Squared moduli $|u_{0,1}|^2$ of radial flow field amplitudes of TVF at mid gap versus relative distance μ of the Reynolds number R_1 from the respective onset in different pure axial magnetic fields $0 < s_z < 0.5$. Inset shows the slope δ of $|u_{0,1}|^2$ versus s_z. Further control parameters are $R_2 = -50$, $k = 3.1415$, and $\eta = 0.5$.

sal field stimulates also additional modes with higher mode-index combinations as indicated in Fig. 3.

Comparing the moduli $|u_{m,1}|$ of the mode amplitudes for $m \in \{0, 1\}$ at the same relative distance μ (3.1) from the respective onset in the differently oriented **H**-fields of Fig. 4 we found the following relations to hold for wTVF and TVF $|u_{m,1}(s_x = c = s_z)| \geq |u_{m,1}(s_x = c, s_z = 0)| \geq |u_{m,1}(s_x = 0, s_z = c)| \geq |u_{m,1}(s_x = 0 = s_z)|$. Here $c = const. \in [0, 1]$.

Summarizing the main results of the bifurcation diagrams presented in Figs. 4 and 5 one can say: In the case $s_x \neq 0$ of a finite transversal field, [(c), (d)], there exist no pure TVF and SPI solutions anymore. Both, for (w)TVF as well as for (w)SPI we found a typical square-root forward bifurcation of the leading mode amplitude. The slope of its square grows with the applied fields.

4. Slope of TVF bifurcation branch in axial fields

Here we first discuss the phenomenon of growing slopes with growing magnetic field in more detail for a pure axial magnetic field. In Fig. 6, this effect is shown in the range $0 < s_z < 0.5$ for the square $|u_{0,1}|^2$ of the leading mode of TVF at $R_2 = -50$. Note, that in this field configuration the pure structure, here TVF, remains unchanged. In order to have a better possibility for comparison we plotted $|u_{0,1}|^2$ in Fig. 6 against the relative distance μ of the Reynolds number R_1 from the onset in the corresponding field. Increasing the field parameter s_z causes the slope $\delta = \partial |u_{0,1}^2| / \partial \mu$ to increase. These slopes are shown in the inset of Fig. 6 versus s_z. An increase of δ has recently been seen also in experimental TVF [47].

5. Bifurcation branches in transversal fields

Here we investigate in more detail the changes of the bifurcation branches of the different vortex structures that are induced by a transversal **H**-field. To that end we show in Fig. 7 reduced moduli $|u_{m,1}(s_x; \mu) / u_{m,1}(s_x = 0; \mu)|$ versus
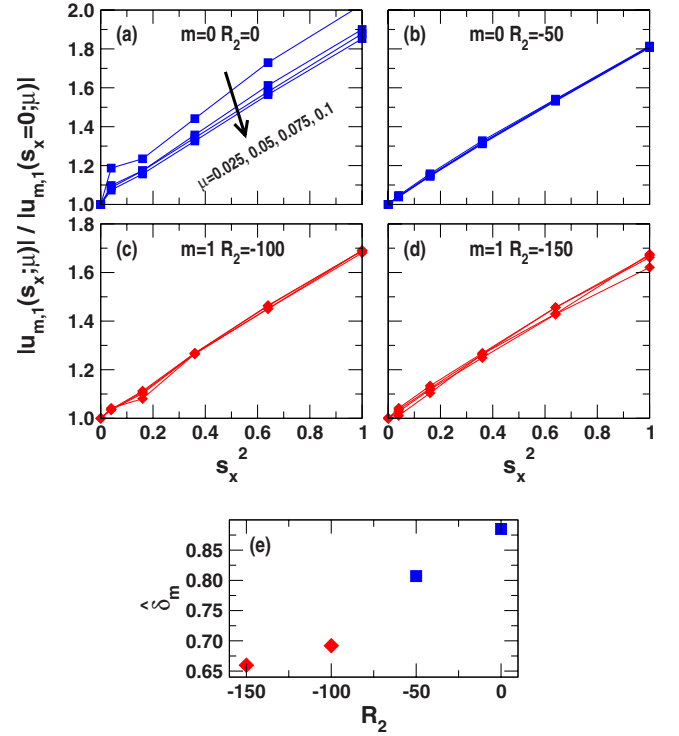

FIG. 7. (Color online) Influence of transversal fields on the nonlinear bifurcation behavior of wTVF and wSPI. In (a)-(d) reduced mode amplitudes $|u_{m,1}(s_x; \mu) / u_{m,1}(s_x = 0; \mu)|$ are shown versus s_x^2 for different supercritical values of $\mu = 0.025$, 0.05, 0.075, 0.1, and R_2 values as indicated. Here ■ ($m = 0$) refers to wTVF and ♦ ($m = 1$) to wSPI, respectively. Further parameters are $k = 3.1415$ and $\eta = 0.5$. In (e) the slopes $\hat{\delta}_m$ of the curves in (a)-(d) are shown versus R_2.

s_x^2 for some selected supercritical values of μ. Here (a) and (b) show wTVF ($m = 0$) while (c) and (d) refer to wSPI ($m = 1$). For wTVF as well as for wSPI and for all values of μ between 0.025 and 0.1 shown in Fig. 7 these ratios are roughly the same for any given s_x. Furthermore, all of them grow practically linearly with s_x^2. The slopes $\hat{\delta}_m = \partial |u_{m,1}(s_x; \mu) / u_{m,1}(s_x = 0; \mu)| / \partial s_x^2$ of the curves in Figs. 7(a)–7(d) are presented in (e) versus the corresponding R_2 values. The slopes $\hat{\delta}_m$ decrease when R_2 becomes more negative.

The fact that $\hat{\delta}_{m=0} > \hat{\delta}_{m=1}$ implies that the reduced wTVF amplitude grows more strongly with the transversal field than the wSPI. In that sense, the influence of transversal **H**-fields on the nonlinear bifurcation behavior is larger for wTVF than for wSPI. On the other hand, the linear bifurcation thresholds of helical wSPI are more strongly shifted by the transversal magnetic field than the onsets of toroidally closed wTVF, c.f. Secs. III C and III D.

B. Vortex structures and mode contents

After having investigated in Sec. III A the changes that differently oriented magnetic field cause in the bifurcation behavior of TVF and SPI we now address structural changes of the vortices and the associated changes in the mode con-
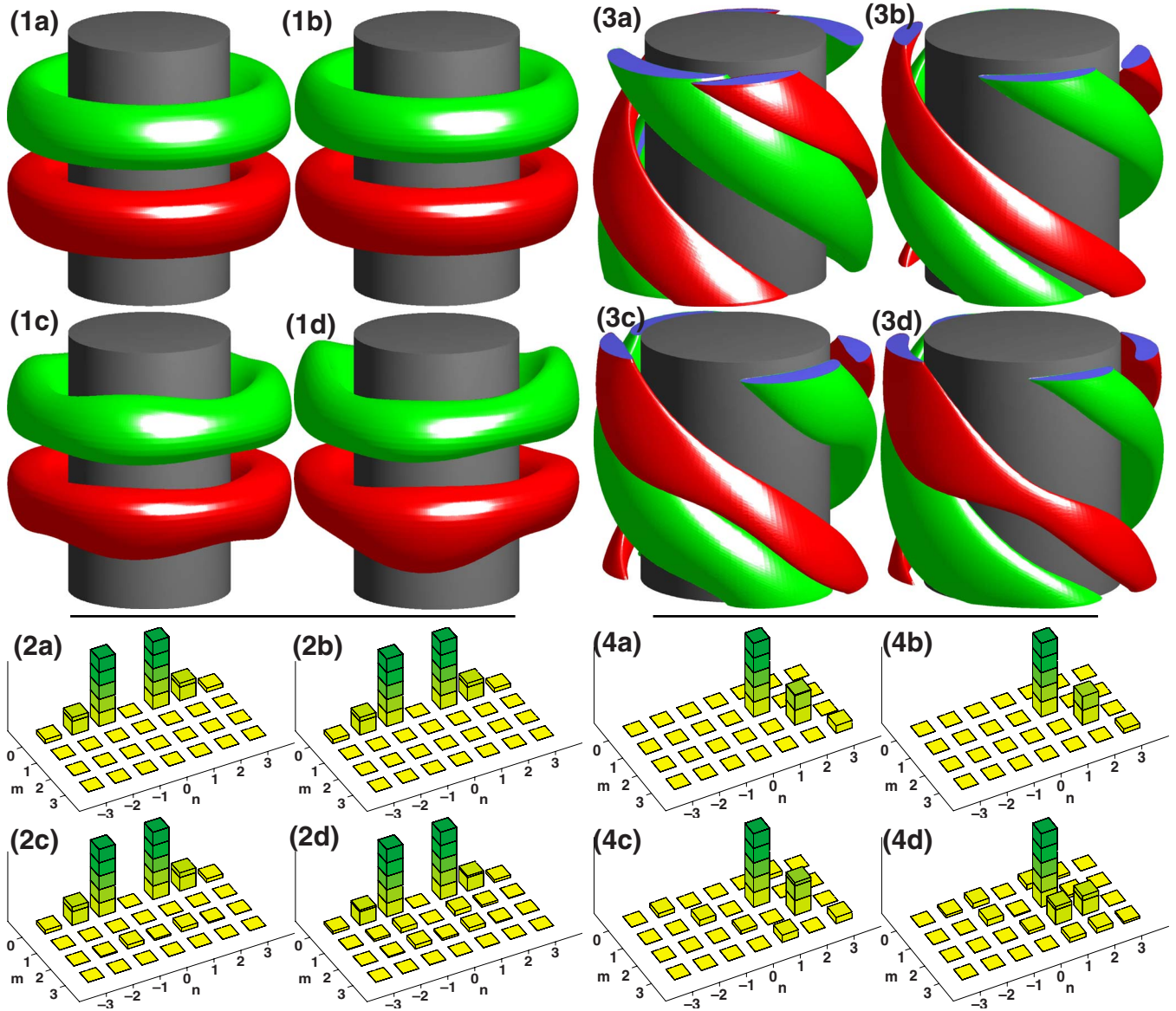
FIG. 8. (Color online) Influence of differently oriented magnetic fields on vortex structures (1, 3) and on the mode contents of the flow (2, 4). In (1, 3) we show iso-surfaces of the azimuthal vorticity $\partial_z u - \partial_r w$ at values ± 90 (1) and ± 70 (2), respectively. For better visibility the 3D vortex structures are plotted in a 4π cylinder with an axial extension of one wavelength. Red (dark gray) refers to positive vorticity and green (light gray) to negative vorticity. In (2, 4) the mode amplitudes $|u_{m,n}|$ of the radial velocity field corresponding to the structures of (1, 3) are shown over the $m-n$ plane. The magnetic field is zero in (a). It is oriented axially in (b) ($s_x=0, s_z=0.6$), transversely in (c) ($s_x=0.6, s_z=0$), and obliquely in (d) ($s_x=0.6=s_z$). So, (a, b) in (1, 2) show TVF, (c, d) in (1, 2) show wTVF, (a, b) in (3, 4) show SPI, and (c, d) in (3, 4) show wSPI. The vortex structures and the magnetic field parameters in (a)-(d) correspond to those of Figs. 4 and 5. Control parameters are $R_1=150, R_2=0$ in (1, 2) and $R_1=160, R_2=-150$ in (3, 4) furthermore $k=3.927$ and $\eta=0.5$.

tents of the flows. So, we discuss here the TVF and wTVF solutions the bifurcation behavior of which have been documented in Fig. 4 for differently oriented fields and similarly for the SPI and wSPI states of Fig. 5.

To visualize the field induced changes in the 3D vortex structures we use in Fig. 8 isosurfaces of the azimuthal vorticity. These surfaces appropriately convey structural details of the vortex flows in question [35]. In Fig. 8 we identify with (a)–(d) the vortex structures and the magnetic fields of Figs. 4 and 5. Thus, (1a) and (3a) in Fig. 8 show TVF and SPI, respectively, without magnetic field while (1b) and (3b)

show them in an axial field. In (1c) and (3c), wTVF and wSPI are shown in a pure transversal field whereas (1d) and (3d) show them in an oblique field.

1. Axial field

A pure axial field (b) does not change the structure of TVF and SPI in real space nor the mode structure of the flow in the $m-n$ Fourier plane. TVF is still made of toroidally closed, rotationally symmetric vortex tubes with a mode spectrum containing only $m=0$ modes. And also the helically oriented, open vortex tubes of the left winding spiral

(L-SPI) shown in Fig. 8(3a) are not changed by an axial field. This also holds for its mirror image the right winding spiral (R-SPI) as well. The SPI flow is periodic in φ, z, and t, say, with axial wave number k, azimuthal wave number M $=1$ in our case, and frequency ω. Furthermore, it does not depend on φ, z, t separately but only on the combined phase variable $\phi = M\varphi \pm kz - \omega t$. Here the +sign refers to a L-SPI and the -sign to a R-SPI. The frequencies of L- and R-SPI are the same and that holds also in the presence of an axial magnetic field. Thus, a pure axial magnetic field does not break the continuous symmetry $f(r, \varphi, z, t) = f(r, \phi)$ of the SPI fields and the mirror symmetry degeneracy of L- and R-SPI, c.f. [48].

2. Transversal and oblique fields

However, the TVF and SPI structures are changed by the presence of a magnetic field with a finite transversal component, $s_x \neq 0$, as shown in (c) and (d), respectively. The isosurfaces become wavy-like deformed and additional modes are stimulated as described in Sec. II E and shown there already schematically in Fig. 3. Thus, a transversal magnetic field (c) generates in wTVF $m = 2$ modes besides the $m = 0$ TVF modes and in wSPI it excites modes $m = n + 2$ on the secondary diagonal in addition to the $m = n$ SPI modes on the diagonal. An oblique field (d), causes beyond the just mentioned modes also $m = 1$ in wTVF and $m = n + 1$ in wSPI.

The spatiotemporal properties of the wTVF that appears in Fig. 8 in transversal and in oblique magnetic fields differ from those of the classic wTVF. In the latter the axial stack of vortex tubes is wavelike bent axially upwards and downwards as a whole. Then, this deformation structure of the vortices rotates as a whole.

A magnetic field with a finite transversal component, on the other hand, deforms the toroidally closed vortices in a different way. Figures 8(1c) and 8(1d) show that the tubes of isosurfaces of the azimuthal vorticity remain for certain φ positions nearly unchanged in comparison with the TVF tubes. However, at other φ positions the deformation is stronger such that their thickness is alternatingly large and small. These thickness deformations are azimuthally somewhat localized and, most importantly, they do not rotate in contrast to the deformation wave of the classic wTVF.

Compared to wTVF the vortices of the wSPI do not show such significant topological differences to the ones without imposed magnetic field. Here, the wavylike deformations look similar. The wSPI as well as the SPI structures rotate already without magnetic field and that remains so in the presence of magnetic fields. More details are discussed in Sec. III F.

C. Intersection of SPI and TVF bifurcation thresholds

A point of special interest in the $R_1 - R_2$ phase plane is the point of higher co-dimension, γ, where the bifurcation thresholds of the primary vortex solutions cross, i.e., of those which branch out of the CCF state. That is here TVF and SPI for axial or zero magnetic fields and wTVF and wSPI for oblique and transversal fields. At γ the order with which these vortex states appear on increasing R_1 changes and with
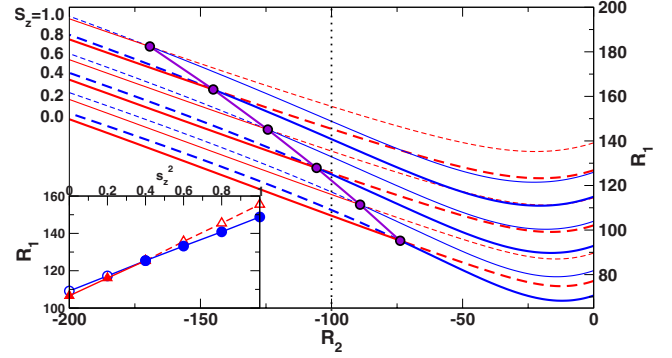

FIG. 9. (Color online) Influence of an axial magnetic field on the location of the bifurcation thresholds of TVF and SPI out of CCF in the $R_2 - R_1$ plane. The field parameters s_z are indicated in the upper left. Further parameters are $k = 3.1415$ and $\eta = 0.5$. Blue (dark gray) lines refer to TVF and red (light gray) ones to SPI. Full (dashed) lines indicate that the bifurcating vortex solution is stable (unstable) at threshold. The line connecting the points shows how the magnetic field shifts the point of higher co-dimension γ. The dotted vertical line marks the fixed R_2 value for the inset. It shows the thresholds as functions of s_z^2.

it the stability of the nonlinear solutions at onset. For example, at moderate R_2 TVF bifurcates first and is stable at onset while SPI bifurcate only later at larger R_1 being unstable at threshold. Order and stability properties are interchanged between these two when R_2 becomes sufficiently negative. This holds also for wTVF and wSPI in oblique and transversal fields.

In Fig. 9, we show as an example the influence of different axial **H**-fields ($0 \leq s_z \leq 1.0$) on the bifurcation thresholds for TVF and SPI and on the location of the γ point. These results of linear calculations were obtained with a shooting method [14]. The blue (dark gray) curves represent the marginal stability boundaries of CCF against onset of TVF and the red (light gray) those for the SPI bifurcation thresholds. Full (dashed) lines indicate that the bifurcating vortex solution is stable (unstable) at threshold.

Increasing s_z stabilizes the ground state CCF, both, against TVF and SPI–c.f. the upwards shift of the respective threshold curves in Fig. 9. But the strength of the stabilization effect is larger for SPI than for TVF so that the point γ moves toward more negative R_2, i.e., to the left in Fig. 9. So, with increasing field parameter s_z the R_2-region of primary, stably bifurcating TVF increases. The magnitude of the shift is bigger for a pure axial **H** field than for a pure transversal **H** field. As an aside we mention that we checked these linear stability results against fully nonlinear simulations of the bifurcating vortex states finding the same behavior.

The inset in Fig. 9 displays the bifurcation thresholds for fixed $R_2 = -100$ versus s_z^2. The change in the sequence of bifurcation and stability by increasing the axial magnetic field is shown. For small to moderate field parameters, say, $0 \leq s_z \leq 0.37$ TVF is the primary stable bifurcating structure while SPI bifurcate secondarily and unstable. For stronger fields, $s_z > 0.37$, the structures interchange stability and bifurcation order.

To summarize: for fixed R_2 an axial field shifts the onset of helical SPI more strongly than the one of toroidally closed
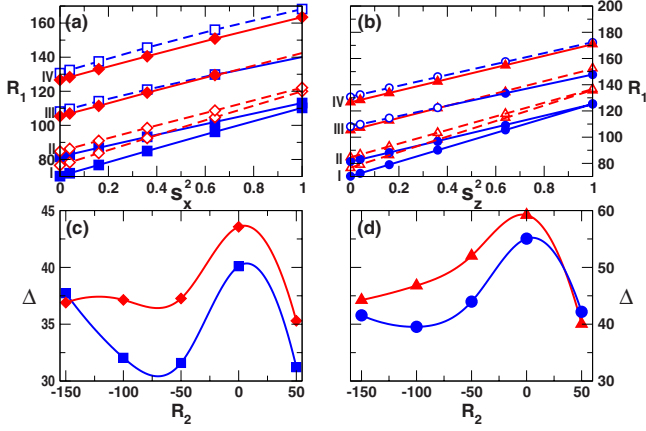
FIG. 10. (Color online) Stabilization of the basic CCF state by pure transversal and pure axial magnetic fields. (a) Bifurcation thresholds $R_{1,bif}$ of vortex structures versus s_x^2 in transversal magnetic fields for $R_2=0$(I), -50(II), -100(III), and -150(IV). (b) $R_{1,bif}$ for axial magnetic fields versus s_z^2 for the same R_2 values as in (a). The slopes $\Delta(R_2)$ (3.2) of the curves in (a) and (b) are shown in (c) and (d), respectively, versus R_2 for the bifurcating structures independent of their stability. Full (dashed) lines with filled (open) symbols denote stable (unstable) bifurcating vortex structures: TVF($\bullet$), SPI ($\blacktriangle$), wTVF ($\blacksquare$), and wSPI ($\blacklozenge$). The results were obtained from non-linear calculations with $k=3.927$ and $\eta=0.5$.

TVF. We furthermore found this behavior also for all parameters and all magnetic field combinations—axial, transversal, and oblique—for which we investigated (w)TVF and (w)SPI.

D. Stabilization of the CCF basic state

In Fig. 9 we already presented the shift of the higher co-dimension point γ and the stabilization of CCF in a pure axial magnetic field resulting from a linear stability analysis done for $k=\pi$. Figure 10(a) presents bifurcation thresholds for vortex flow in pure transversal magnetic fields ($s_x \neq 0, s_z=0$) while Fig. 10(b) shows them for pure axial fields ($s_x=0, s_z\neq0$). These results were obtained by non-linear calculations with the full field equations for $k=3.927$ and different R_2. The upward shifts of the bifurcation values $R_{1,bif}$ shown in Figs. 10(a) and 10(b), i.e., the stabilization of CCF grows linearly with s_x^2 or s_z^2, respectively. This holds for all the bifurcation thresholds of TVF, SPI, wTVF, and wSPI alike. However, the slopes of the curves in Figs. 10(a) and 10(b) differ and they depend on R_2.

All the data presented in Figs. 10(a) and 10(b) on the variation of $R_{1,bif}$ with R_2 and s_i ($i=x$ or z) can be well parameterized by the following formula

$$R_{1,bif}(R_2,s_i) = R_{1,bif}(R_2=0,s_i) + \Delta(R_2)s_i^2. \qquad (3.2)$$

Figures 10(c) and 10(d) shows how the slopes Δ that can be read off from the plots of $R_{1,bif}$ versus s_i^2 in Figs. 10(a) and 10(b) vary with R_2. One can see that Δ is largest in both pure field configurations for $R_2=0$, i.e., the increase of the CCF stabilization with growing s_i is largest for $R_2=0$.

In the whole parameter range $-150 < R_2 < 50$ that we have examined here, a pure transversal field has a weaker influence on the onsets than a pure axial magnetic field since $\Delta(R_2,s_x) < \Delta(R_2,s_z)$. So, while axial fields shift the onsets more strongly than pure transversal ones the latter have a stronger influence on the non-linear spatiotemporal properties of the bifurcating vortex structures.

E. Nonrotating, phase pinned wTVF in magnetic fields

The topological structures of the different vortex solutions were presented in Sec. III B. Here, we focus on the dynamics of the deformations of TVF generated by a transversal or an oblique magnetic field.

The classic wTVF [32–35], arises by deforming the TVF such that the axial stack of closed vortex tubes is wavelike bent axially upwards and downwards as a whole. Then, this deformation structure of the vortices rotates as a whole with a characteristic frequency.

A magnetic field with a finite transversal component, on the other hand, deforms the toroidally closed vortices in a different way as shown in Figs. 8(1c) and 8(1d), c.f. Sec. III B 2. The tubes of iso-surfaces of the azimuthal vorticity remain for certain φ positions nearly unchanged in comparison with the TVF tubes. However, at other somewhat localized φ positions they are swollen and at others they are constricted. This pattern of thickness variations is azimuthally pinned and does not rotate—the field induced wTVF structure is stationary as the rotationally symmetric TVF. Moreover, transversal and oblique fields show similar behavior, c.f. Figs. 8(1c) and 8(1d). In both cases one observes a stationary wavy Taylor vortex structure. The only difference is the magnitude and the form of the deformation. Oblique fields yield a stronger deformation (see also Fig. 8).

F. Frequencies of SPI and of wSPI structures

The non-rotating, phase pinned wTVF that are generated by a magnetic field evolve out of TVF which being rotational symmetric is stationary. Now it is interesting to see how a magnetic field influences a structure that has already at **H** $=0$ a finite frequency. So, here we investigate how the SPI rotation frequencies and with it the associated axial propagation speeds are changed by different magnetic fields.

In Fig. 11, we show the frequencies $\omega_{1,1}$ of the complex mode amplitudes $u_{1,1}$ of the radial velocity field in the middle of the gap versus reduced distance μ Eq. (3.1) of R_1 from the respective bifurcation thresholds. See Fig. 5 for the corresponding bifurcation diagrams of the moduli $|u_{1,1}|$ of the respective SPI and wSPI solutions.

A first obvious result is that any kind of a magnetic field increases the frequencies. Second, the frequencies of SPI and of wSPI are shifted stronger by an axial than by a transversal field, like their onset shifts. Third, the qualitative bifurcation behavior of SPI and of wSPI, i.e., their variation with μ is basically the same: they all decrease with increasing μ in a similar way. This behavior of the frequencies of the non-linear SPI and wSPI patterns has to be contrasted with the linear SPI frequencies given by the imaginary eigenvalue of linear SPI perturbations of the CCF which tend to increase with growing μ [35,45].
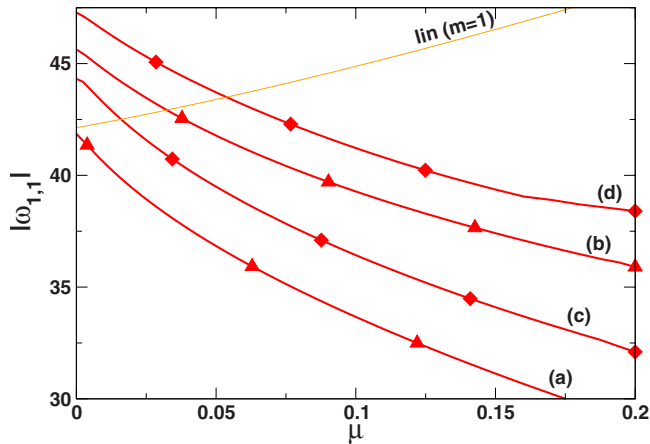
FIG. 11. (Color online) Bifurcation diagrams of the frequencies $\omega_{1,1}$ of the complex mode amplitudes $u_{1,1}$ of the radial velocity field in the middle of the gap versus reduced distance μ Eq. (3.1) of R_1 from the respective bifurcation thresholds. The corresponding bifurcation diagrams of the moduli $|u_{1,1}|$ are shown in Fig. 5. Lines with triangles (lozenges) refer to SPI (wSPI) solutions. The thin line shows the linear spiral frequency ($m=1$) for $\mathbf{H}=0$, i.e., the imaginary part of the SPI eigenvalues of the Navier-Stokes Eq. (2.12) linearized around the CCF state. (a) $s_x=0.0$, $s_z=0.0$; (b) $s_x=0.0$, $s_z=0.6$; (c) $s_x=0.6$, $s_z=0.0$; (d) $s_x=0.6$, $s_z=0.6$. Further parameters are $k=3.927$, $R_2=-150$.

IV. CONCLUSION

We have explored the influences of different magnetic field configurations on the flow of a ferrofluid in the Taylor-Couette system. In particular, we investigated the bifurcation behavior and the spatiotemporal properties of Taylor vortices, wavy Taylor vortices, spiral vortices, and of wavy spiral vortices under the influence of homogeneous magnetic fields that are oriented axially, transversally, or obliquely.

For our numerical calculations, we used an approach analogous to the model of Niklas *et al.* [24,26] that assumes a stationary magnetization near the equilibrium and sufficiently small relaxation times. Depending on the orientation of the applied magnetic field the spatiotemporal structure of TVF and of SPI is in general changed so that additional modes entering the axial and azimuthal Fourier decomposition of the flow are excited. However, the flow structure of TVF and of SPI does not change in real space and in Fourier space when the magnetic field is oriented axially: the symmetry properties are unaffected, only the flow amplitudes

and, in case of SPI, the frequencies are altered by an axial field.

All magnetic fields stabilize the CCF ground state: the bifurcation thresholds for vortex structures are shifted to higher values of the inner Reynolds number R_1. The shifts are linear in both field parameters, s_x^2 and s_z^2. The stabilization by an axial field is stronger than by a transversal one. Furthermore, the onsets of the helical SPI and wSPI are moved more strongly by the fields than those of the toroidally closed TVF and wTVF. The nonlinear SPI and wSPI frequencies increase with growing magnetic field parameters and the frequency shift is largest for axial magnetic fields. But their qualitative bifurcation behavior is similar: they decrease in a similar way with increasing relative distance μ from the onset.

When the magnetic field has a nonzero transversal component then the pure TVF and SPI structures do not exist any more. Instead, the vortex structures that then grow via a primary, forward bifurcation out of CCF are wavily deformed: namely wTVF and wSPI. We presented the spatiotemporal properties and the bifurcation behavior of these wavy structures in different applied magnetic fields. Since we are not aware of previous work neither in theory nor in experiments devoted to transversal or oblique fields we consider our investigations of these wavy structures also as a stimulus for further work, in particular for experiments.

Especially the wavy Taylor vortices generated by a transversal or an oblique field differ crucially from the classic wTVF that bifurcates without magnetic field out of TVF at relatively large R_1 [7,8]. The field generated wTVF, on the other hand, arises via a primary bifurcation directly out of CCF. Furthermore, structure and dynamics of this wTVF are different: (i) The vortex tubes are periodically expanded and constricted in φ direction while in the classic wTVF the axial stack of vortex tubes is wave-like bent axially upwards and downwards. (ii) The field generated deformation pattern is pinned, i.e., stationary as the rotationally symmetric TVF while the classic wTVF structure rotates as a whole with constant frequency.

It would be interesting to compare the effects of different magnetic fields on the bifurcation behavior and the spatiotemporal properties of mhd flows in the Taylor-Couette setup with our findings for ferrofluids.

[1] M. M. Couette, C. R. Acad. Sci. Paris **107**, 388 (1888).
[2] G. I. Taylor, Philos. Trans. R. Soc. London, Ser. A **223**, 289 (1923).
[3] S. Chandrasekhar, *Hydrodynamic and Hydromagnetic Stability* (Dover, New York, 1981).
[4] R. C. DiPrima and H. L. Swinney, in *Hydrodynamic Instabilities and the Transition to Turbulence, No. 45 in Topics in Applied Physics*, edited by H. L. Swinney and J. G. Gollub

(Springer, Berlin, 1985).
[5] C. D. Andereck, S. S. Liu, and H. L. Swinney, J. Fluid Mech. **164**, 155 (1986).
[6] R. Donnelly, Phys. Today **44**(11), 32 (1991).
[7] P. Chossat and G. Iooss, *The Couette-Taylor problem* (Springer, Berlin, 1994).
[8] R. Tagg, Nonlinear Sci. Today **4**(3), 1 (1994).
[9] R. E. Rosensweig, *Ferrohydrodynamics* (Cambridge Univer-

sity Press, Cambridge, England, 1985).

[10] B. M. Berkovsky, V. F. Medvedev, and M. S. Krakov, *Magnetic Fluids: Engineering Applications* (Oxford University Press, Oxford, 1993).

[11] B. M. Berkovsky and V. Bashtovoy, *Magnetic Fluids and Applications Handbook* (Begell House, Inc., New York, 1996).

[12] E. Blums, A. Cebers, and M. M. Maiorov, *Magnetic Fluids* (Walter de Gruyter, Berlin, 1997).

[13] S. Odenbach, *Magnetoviscous Effects in Ferrofluids*, Lecture Notes in Physics Vol. 71 (Springer, Berlin, 2002).

[14] A. Leschhorn, M. Lücke, Ch. Hoffmann, and S. Altmeyer, Phys. Rev. E **79**, 036308 (2009).

[15] R. E. Rosensweig, R. Kaiser, and G. Miskolczy, J. Colloid Interface Sci. **29**, 680 (1969).

[16] J. P. McTague, J. Chem. Phys. **51**, 133 (1969).

[17] W. F. Hall and S. N. Busenberg, J. Chem. Phys. **51**, 137 (1969).

[18] M. I. Shliomis, Sov. Phys. JETP **34**, 1291 (1972).

[19] M. Holderied, L. Schwab, and K. Stierstadt, Z. Phys. B: Condens. Matter **70**, 431 (1988).

[20] O. Ambacher, S. Odenbach, and K. Stierstadt, Z. Phys. B **86**, 29 (1992).

[21] S. Odenbach and H. Gilly, J. Magn. Magn. Mater. **152**, 123 (1996).

[22] M. Reindl, A. Leschhorn, M. Lücke, and S. Odenbach, J. Phys.: Conf. Ser. **149**, 012109 (2009).

[23] A. N. Vislovich, V. A. Novikov, and A. K. Sinitsyn, J. Appl. Mech. Tech. Phys. **27**, 72 (1986).

[24] M. Niklas, Z. Phys. B **68**, 493 (1987).

[25] P. J. Stiles, M. Kagan, and J. B. Hubbard, J. Colloid Interface Sci. **120**, 430 (1987).

[26] M. Niklas, H. Müller-Krumbhaar, and M. Lücke, J. Magn. Magn. Mater. **81**, 29 (1989).

[27] M. H. Chang, C. K. Chen, and H. C. Weng, Int. J. Eng. Sci. **41**, 103 (2003).

[28] J. Singh and R. Bajaj, J. Magn. Magn. Mater. **294**, 53 (2005).

[29] J. Singh and R. Bajaj, Int. J. Math. Math. Sci. **2005**, 3727 (2005).

[30] S. Odenbach and H. W. Müller, Phys. Rev. Lett. **89**, 037202 (2002).

[31] Throughout this paper we use the abbreviations CCF: circular Couette flow TVF: Taylor vortex flow SPI: spiral vortex flow L-SPI: left winding spiral R-SPI: right winding spiral wTVF: wavy Taylor vortex flow wSPI: wavy spiral vortex flow.

[32] M. Golubitsky, I. Stewart, and D. Schaeffer, *Singularities and Groups in Bifurcation Theory II* (Springer, New York, 1988).

[33] M. Golubitsky and W. F. Langford, Physica D **32**, 362 (1988).

[34] M. Golubitsky and I. Stewart, SIAM J. Math. Anal. **17**, 249 (1986).

[35] Ch. Hoffmann, S. Altmeyer, A. Pinter, and M. Lücke, New J. Phys. **11**, 053002 (2009).

[36] M. A. Martsenyuk, Y. L. Raikher, and M. I. Shliomis, Sov. Phys. JETP **38**, 413 (1974).

[37] B. U. Felderhof and H. J. Kroh, J. Chem. Phys. **110**, 7403 (1999).

[38] B. U. Felderhof, Phys. Rev. E **62**, 3848 (2000).

[39] M. I. Shliomis, Phys. Rev. E **64**, 060501 (2001).

[40] M. I. Shliomis, Phys. Rev. E **64**, 063501 (2001).

[41] H. Walter Müller and M. Liu, Phys. Rev. E **64**, 061405 (2001).

[42] A. Leschhorn and M. Lücke, Z. Phys. Chem. **220**, 219 (2006).

[43] A. Leschhorn and M. Lücke, Z. Phys. Chem. **220**, 89 (2006).

[44] A. Leschhorn, J. P. Embs, and M. Lücke, J. Phys.: Condens. Matter **18**, S2633 (2006).

[45] Ch. Hoffmann and M. Lücke, *Physics of Rotating Fluids* (Springer Verlag, Berlin, 2000), Vol. 549, p. 55.

[46] Ch. Hoffmann, M. Lücke, and A. Pinter, Phys. Rev. E **72**, 056311 (2005).

[47] M. Reindl and S. Odenbach (private communication).

[48] A. Pinter, M. Lücke, and Ch. Hoffmann, Phys. Rev. Lett. **96**, 044506 (2006).